Photodiagnosis and Photodynamic Therapy 29 (2020) 101600

Contents lists available at ScienceDirect

Photodiagnosis and Photodynamic Therapy

journal homepage: www.elsevier.com/locate/pdpdt

Investigating the mechanisms behind extensive death in human cancer cells following nanoparticle assisted photo-thermo-radiotherapy

Mohammad Mehdi Movahedi[a,b,1], Zahra Alamzadeh[a,c,1], Samira Hosseini-Nami[c], Ali Shakeri-Zadeh[c,d], Gholamreza Taheripak[e], Amirhossein Ahmadi[f], Arash Zare-Sadeghi[c], Habib Ghaznavi[g,*], Alireza Mehdizadeh[a,b,**]

[a] Department of Medical Physics and Medical Engineering, School of Medicine, Shiraz University of Medical Sciences, Shiraz, Iran
[b] Ionizing and Non-Ionizing Radiation Protection Research Center (INIRPRC), Shiraz University of Medical Sciences, Shiraz, Iran
[c] Finetech in Medicine Research Center, Iran University of Medical Sciences (IUMS), Tehran, Iran
[d] Medical Physics Department, School of Medicine, Iran University of Medical Sciences (IUMS), Tehran, Iran
[e] Clinical Biochemistry Department, School of Medicine, Iran University of Medical Sciences (IUMS), Tehran, Iran
[f] Pharmaceutical Sciences Research Center, Faculty of Pharmacy, Mazandaran University of Medical Sciences, Sari, Iran
[g] Zahedan University of Medical Sciences (ZaUMS), Zahedan, Iran

ARTICLE INFO

Keywords:
Cancer nanotechnology
Combination therapy
Cell morphology
Molecular change
Apoptosis

ABSTRACT

We have recently reported the synthesis and characterization of gold-coated iron oxide nanoparticle and demonstrated such a nanoparticle ($Au@Fe_2O_3$ NP) was able to significantly enhance the lethal effects of photo-thermo-radiotherapy. The purpose of this study was to determine the mechanisms behind such an enhancement by investigating the changes induced in cancer cell viability, proliferation, and morphology as well as monitoring the alteration of some genes which play important role in the process of cell death. Using MTT assay and transmission electron microscopy (TEM), the KB cells viability and morphology were assessed after treating with various combinations of NPs, photothermal therapy (PTT), and radiotherapy (RT). Clonogenic assay was used to assess the proliferation ability of treated KB cells. Nanoparticle internalization into the cells was investigated by TEM and inductively coupled plasma (ICP). During the treatment procedures, temperature changes were monitored using an IR-camera. Furthermore, the changes occurred in Bax, BCL2 and HSP70 genes expression level were measured using real-time PCR. The results showed that combination of NP, PTT, and RT caused more cell death compared to PTT or RT alone. Following such a combination therapy, massive cell injury was detected. We also observed an extensive increase in Bax/Bcl2 ratio and HSP70 expression for the KB cells treated by combination therapy procedure. Our results showed that massive cell injury and apoptosis induction are the main reasons of extensive cell death observed in cancer cells when a nanoparticle assisted photo-thermo-radiotherapy procedure is applied.

1. Introduction

Surgery, chemotherapy and radiotherapy (RT) are common cancer treatments and each suffers from certain limitations [1]. One of the challenges of RT is that ionizing radiation affects not only cancer cells but also normal tissues [2]. Therefore, the presence of critical organs in the vicinity of a tumor is a limiting factor for the administration of a sufficient dose [3]. One way to overcome this limitation is the use of radiosensitizers. For example, nanoparticles (NPs) with high atomic number (Z) can be used and aggregated in cancer cells as radiosensitizing agents and consequently the radiation absorbed dose is increased [2,4–6]. Another problem with RT, which increases the risk of tumor relapse, is the presence of hypoxic cells in tumors [7]. Nanoparticle assisted photothermal therapy (PTT) procedures have been recently introduced as an efficient method to sensitize the hypoxic tumors. As the photosensitizing agents, the NPs are introduced into the cancer cells and then are illuminated with an appropriate laser [8]. The electrons of NPs absorb the energy of laser and rapidly vibrate. This phenomenon is called the surface plasmon resonance (SPR) in which laser light energy is converted to heat [9]. As a result, temperature of a

* Corresponding author at: Zahedan University of Medical Sciences (ZaUMS), Zahedan, Iran.
** Corresponding author at: Department of Medical Physics and Medical Engineering, School of Medicine, Shiraz University of Medical Sciences, Shiraz, Iran.
E-mail addresses: dr.ghaznavi@zaums.ac.ir (H. Ghaznavi), mehdizade@sums.ac.ir (A. Mehdizadeh).
[1] Theses authors (MMM & ZA) contributed equally to this work.

https://doi.org/10.1016/j.pdpdt.2019.101600
Received 10 August 2019; Received in revised form 29 October 2019; Accepted 8 November 2019
Available online 13 November 2019
1572-1000/

tumor is expected to be increased and consequently the vascular permeability is changed. Finally, the blood flow and oxygen level inside the tumor are increased. Also, structural changes in cancer cells such as membrane rupture and protein denaturation are occurred and ultimately apoptosis can be highly induced [10].

Considering all stated above, it can be stated that the combination of RT and PTT has synergistic effects and such a combination in the presence of NPs can improve cancer treatment procedures [11]. We have recently reported the synthesis and characterization of gold-coated iron oxide core-shell NPs and demonstrated such a nanoparticle ($Au@Fe_2O_3$ NP) is able to significantly enhance the lethal effects of photo-thermo-radiotherapy [12]. Each of these nanoparticles (gold or iron oxide nanoparticle) has its own advantages. In addition to its high potentials in magnetic resonance imaging of cancer cells, it has been demonstrated iron oxide NPs can be efficiently used in the process of cancer photothermal therapy [13]. Moreover, iron oxide NPs can induce DNA damage, necrosis, and apoptosis [14]. On the other hand, gold nanoparticle (AuNP) is an inert and biocompatible nanostructure and it is an ideal sensitizing agent for PTT and RT because of its unique optical properties and high atomic number [5,15].

Considering the unique properties of both AuNPs and iron oxide NPs, it would be desirable to have these two NPs in a single nanostructure such as $Au@Fe_2O_3$ core-shell NPs. As stated earlier, we have recently demonstrated $Au@Fe_2O_3$ NP is able to significantly enhance the lethal effects of photo-thermo-radiotherapy [12]. The purpose of this study is to describe the mechanism behind such an enhancement by monitoring the changes induced in cancer cell morphology and the alteration of some genes after an $Au@Fe_2O_3$ NP assisted photo-thermo-radiotherapy procedure. In the current study, the combinatorial effects of megavoltage X-ray and PTT in the presence of $Au@Fe_2O_3$ NPs were studied on KB human nasopharyngeal cancer cells. The reason for choosing KB cells was that the nasopharynx was surrounded by vital organs such as the brainstem, spinal cord, temporal lobes, eyes, ears, and parotid glands. Therefore, radiotherapy of nasopharyngeal carcinoma is facing big challenges and the results of treatment are not satisfactory [16,17]. As a solution, here, we suggest the application of $Au@Fe_2O_3$ core-shell NPs assisted PTT prior to RT. In addition to KB cancer cells, we also examined the effects of $Au@Fe_2O_3$ NPs on human gingival fibroblast (HGF) cells, as the healthy model which is frequently used for head and neck studies.

2. Materials and methods

2.1. Materials

Gold-coated iron oxide $Au@Fe_2O_3$ nanoparticles were prepared as reported previously [12]. Trypsin ethylenediaminetetraacetic acid (EDTA), fetal bovine serum (FBS), streptomycin and penicillin were purchased from Gibco®. Dimethylsulfoxide (DMSO), 3- (4,5-dimethylthiazol-2-yl) -2,5-diphenyltetrazolium bromide (MTT), phosphate buffered saline (PBS), crystal violet, trypan blue were purchased from Sigma-Aldrich, USA. Dulbecco's culture medium with Modified Eagle's Medium (DMEM) was purchased from Biowest, France. A high purity RNA isolation kit, a first strand synthesis kit and the PCR Master Mix Green were manufactured by Roche (Germany), Gene All (Korea) and Ampliqon (Denmark), respectively. The primers were synthesized by Sinaclon (Teheran, Iran). The KB and HGF cell lines were obtained from the Pasteur Institute of Iran (Tehran, Iran).

2.2. Characterization of $Au@Fe_2O_3$ core-shell NP

Morphological properties of the synthesized NPs were analyzed with a Zeiss LEO 906 transmission electron microscope (TEM). The protocol of TEM studies was according to what we have reported previously [12]. Also, hydrodynamic size distribution and zeta potential of the synthesized NPs were determined using a Malvern Zetasizer, NANO ZS (Malvern Instruments Limited, UK).

2.3. Cell culture and cytotoxicity assay

Our experiments were performed on KB cells (derived from cancer of the epidermis in the mouth of a Caucasian adult male). The KB cells were cultured in DMEM culture medium supplemented with 10 % FBS, 1 % penicillin-streptomycin solution to reduce the risk of microbial contamination in cell culture, and then maintained in an incubator (5 % CO_2; 37 °C).

KB cells were seeded in 96 well plate at concentration of 10^4 cells in 100 µL culture medium. The plate was incubated for 24 h so that the cells adhere to the plate and their confluence reaches 70–80%. Then, different concentrations of NPs (50, 100, 150 µM) were added to the cells. After 4 h of incubation, the NPs were washed twice with PBS and fresh culture medium with FBS was added to the cells and incubated for 24 h. Cell viability was measured by MTT assay as described in our previous publication [12]. Also, as the control group, NPs biocompatibility were studied on HGF normal cell line.

To assess the effect of laser, cells incubated with NPs for 4 h and then exposed by 808 nm laser for 5 min (2 W/cm^2). The effects of NPs on temperature rise profile of the cells irradiated by laser were monitored by an IR camera (Testo 875–1i, Germany).

Also, the role of RT in combination with laser and NPs was studies by exposing the cells, treated in previous section, to 6 MV X-ray at the doses of 2 and 4 Gy (dose rate: 2 Gy/min). Twenty four hours post treatment, the viability of KB cells was measured using MTT assay as described in our previous publication [12].

2.4. Cellular uptake assessments

Nanoparticle cell uptake was investigated using two different methods; inductively coupled plasma mass spectrometry (ICP-MS) and transmission electron microscopy (TEM). The KB cells were cultured in two wells of 6-well plate (300,000 cells/well). After 24 h, the NPs were incubated with the adhered cells for 4 h. Then, the cells were washed with PBS, collected using trypsin, and finally centrifuged. In this step, two separate cell pellets were obtained. One of the cell pellets was dissolved in aqua regia and examined for the Au content by ICP-MS (ELAN DRC-e spectrometer; PerkinElmer SCIEX, Concord, Ontario, Canada). Another sample of cell pellet was fixed with glutaraldehyde fixative and was examined by TEM to visualize the process of NPs cell uptake.

2.5. Study of ultrastructure changes of treated cells

TEM study was performed to study the ultrastructure changes of KB cells. The effect of combination therapy (NPs + Laser + RT) on treated KB cells was compared with untreated cells. After treating the KB cells with combination therapy method, they were washed with PBS, collected by centrifugation and then studied using a protocol reported previously [18].

2.6. Clonogenic assay

For clonogenic assay, the KB cells were incubated in 60 mm dishes with and without NPs for 4 h. Then, the cells were irradiated with 6 MV X-ray at different doses (0, 2, 4 and 6 Gy). The dishes were kept in incubator for 10 days. The cells were then stained with crystal violet and colonies were counted. Plate efficiency (PE) and surviving fraction (SF) were calculated using the following formula:

$$PE = \frac{\#\ of\ colonies\ formed}{\#\ of\ cells\ seeded} \times 100$$

Table 1
Oligo sequences used in the present study.

Primer name	Oligo sequences
Bax, Forward	CAAACTGGTGCTCAAGGCCC
Bax, Reverse	GAGACAGGGACATCAGTCGC
Bcl2, Forward	CAGGATAACGGAGGCTGGGATG
Bcl2, Reverse	GACTTCACTTGTGGCCCAGAT
HSP70, Forward	GTGCATTGCAGTGTGCCATC
HSP70, Reverse	GGGCAAATCCTGAGGAGAGC
Actin β, Forward	ACAGAGCCTCGCCTTTGCC
Actin β, Reverse	GATATCATCATCCATGGTGAGCTGG

$$SF = \frac{\#\ of\ colonies\ formed\ after\ treatment}{\#\ of\ cells\ seeded\ \times PE/100}$$

2.7. Quantitative real- time PCR (qRT- PCR)

Changes in gene expression were assessed by qRT-PCR. The KB cells were cultured in 48-well plates at a concentration of 70,000 cells in 250 µL of DMEM culture medium. The cells were incubated for 24 h until they adhered to the plate. As described above, the cells received various treatments and then qRT-PCR was performed to determine the changes in expression levels of Bax, Bcl2, and HSP70 genes (Table 1).

First, RNA extraction was performed according to the protocol of Roche's high purity RNA isolation kits. The concentration, purity and integrity of the RNA were measured with a nanodrop (Thermo Scientific, USA). The RNA was reverse transcribed to cDNA using the first strand synthesis kit (GeneAll, Biotech, Korea). The obtained cDNA was subjected to qRT-PCR using primers directed by Bax, Bcl2 and HSP70. Actin β was used as a house keeping gene. The reaction mixture was prepared according to PCR Master Mix Green, (Ampliqon, Denmark). QRT-PCR was performed with the real-time PCR StepOne (48-well) from Applied Biosystems, USA, with a standard thermal profile. The transcriptional modifications were calculated by the Delta-Ct method and normalized with the house keeping gene. The averages were obtained from triplicate samples.

2.8. Statistical analysis

All experiments were done at least three times. One-way ANOVA followed by Tukey's test as the post-hoc analysis was done for statistical analysis using SPSS version 16. The value of $p < 0.05$ was considered to be statistically significant. Also, correlations between cell death and gene expressions were assessed by Pearson correlation coefficient. All data are reported as the mean values ± SE (standard error).

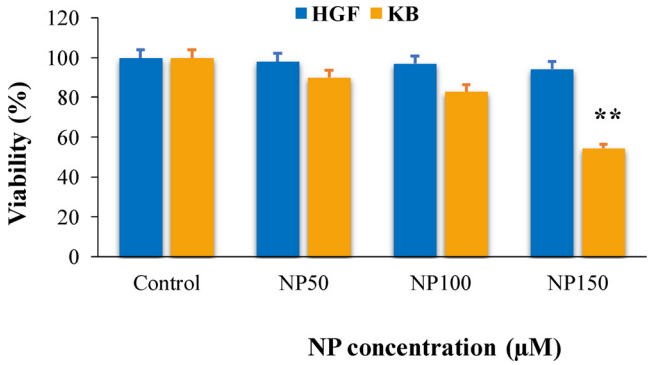

Fig. 2. The viability of HGF and KB cells incubated with different concentrations of NPs (data are shown as the Mean ± SE, ** means P- value < 0.001).

3. Results

3.1. Characterization of nanoparticles

TEM image of $Au@Fe_2O_3$ core-shell NPs is shown in Fig. 1. The core-shell structure and spherical shape are obvious in this Figure. The hydrodynamic size distribution of the synthesized NPs was studies and we observed the NPs were ranged from 40 to 60 nm. Also, Zeta potential analysis showed the synthesized NPs were negatively charged (-19.7 mV), indicating an appropriate stability of NPs.

3.2. Cytotoxicity of $Au@Fe_2O_3$ NPs

To evaluate the cytotoxic effects of the NPs, KB and HGF cells were incubated with different concentrations of NPs. The results of MTT assay showed that KB cell viability decreased in the presence of NPs (Fig. 2). Higher concentrations of NPs led to more cell death. At the highest concentration (150 µM), KB cell viability decreased to 54.41 %, while at the concentrations of 50 and 100 µM, cell viability was 90.12 % and 83.08 %, respectively. The statistical analysis showed such a cell death due to NPs incubation were significant in comparison to the control group ($p < 0.001$). Also, it was showed that the core-shell NPs had no significant toxicity on normal cells even at higher concentration.

3.3. Effects of PTT

Fig. 3 shows the results of our studies to determine the PTT effects. The viability of KB cells received the laser beam alone was 94.71 %. The cells were also incubated with various concentrations of NPs for 4 h and then received laser irradiation. MTT results showed that viability of the

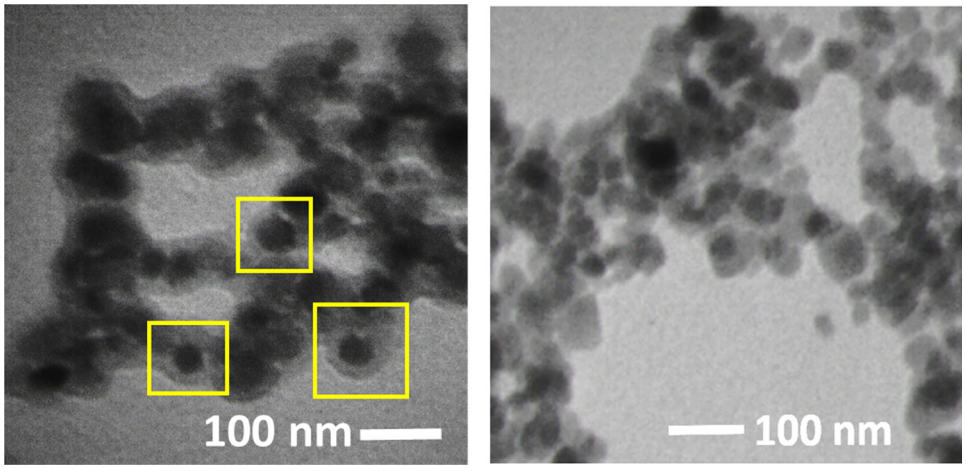

Fig. 1. Transmission electron microscopy (TEM) images of the synthesized $Au@Fe_2O_3$ NPs. Core-shell structure can be easily seen in yellow squares.

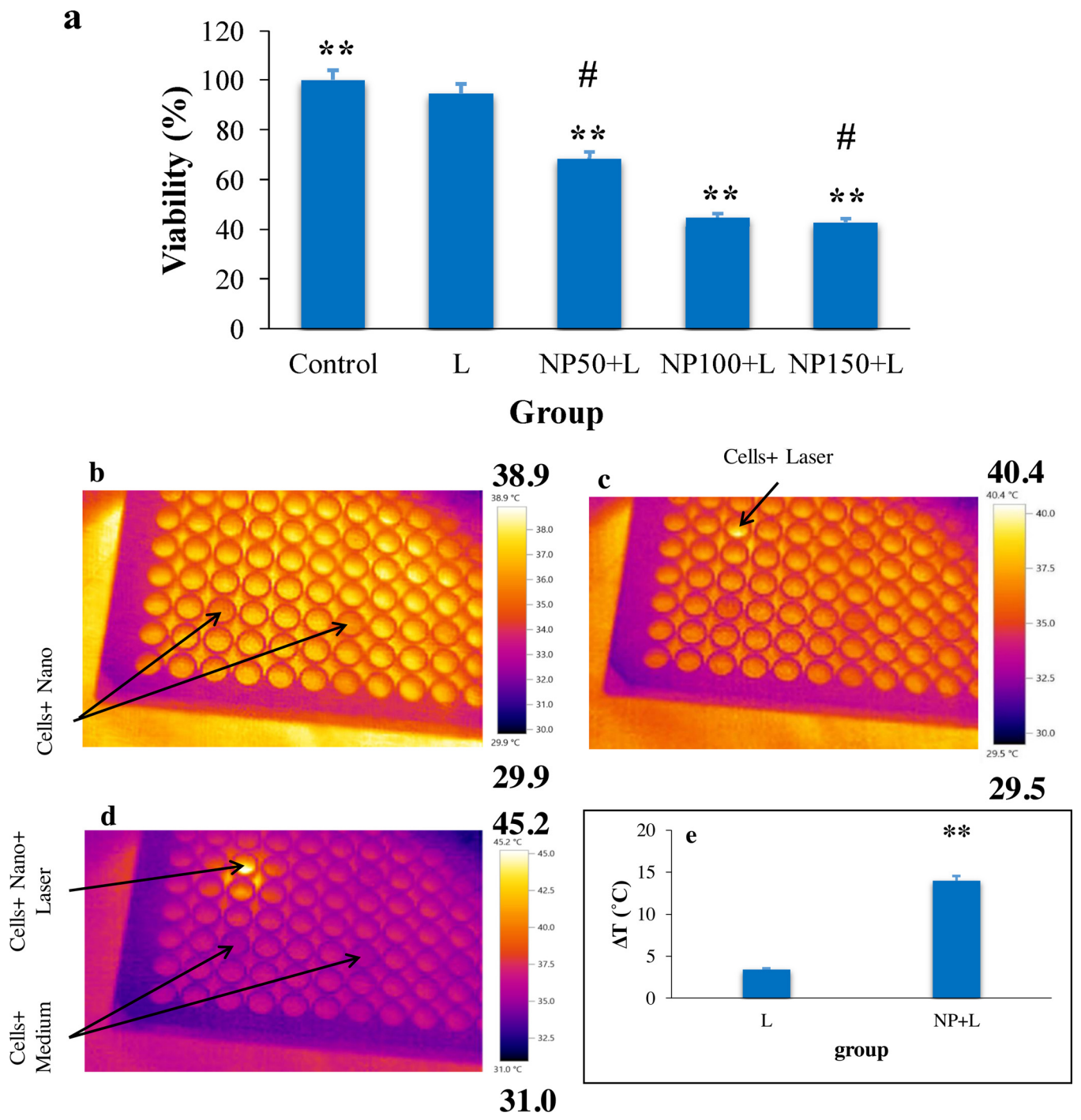

Fig. 3. (a) KB cell viability incubated with different concentrations of NPs for 4 h and then irradiated by laser. Data are shown as the Mean ± SE. "L" stands for laser group. (** and # show P- value < 0.001). Temperature distribution maps of KB cells treated by (b) NPs, (c) laser, and (d) NPs + L are also shown in this figure. Part (e) shows thermal changes in KB cells treated by laser and the combination of laser + NPs.

cells incubated with NPs and exposed to the laser was significantly less than the viability of the cells treated with laser alone ($P < 0.001$). Also, temperature distribution maps of KB cells treated by NPs, laser, and the combination of NPs + Laser are shown in Fig. 3. As it is obvious in Fig. 3(e), we found that there was a significant difference between temperature change (ΔT) in the KB cells treated by laser and the combination of NP + laser.

3.4. Effects of photo-thermo-radiotherapy

In this section of our studies, the effect of combination therapy on KB cells was assessed. As shown in Fig. 4, photo-thermo-radiotherapy in the presence of NPs caused significant cell death compared to other modalities such as RT alone or RT + Laser. Also, it was found that the NPs concentration had a significant effects on cell viability when applied in the process of photo-thermo-radiotherapy.

3.5. Cellular uptake

TEM images presented in Fig. 5 (a) indicate the presence of NPs inside the KB cells mitochondria and cytoplasm. ICP-MS test was also confirmed the entrance of NPs into the KB cells by measuring the

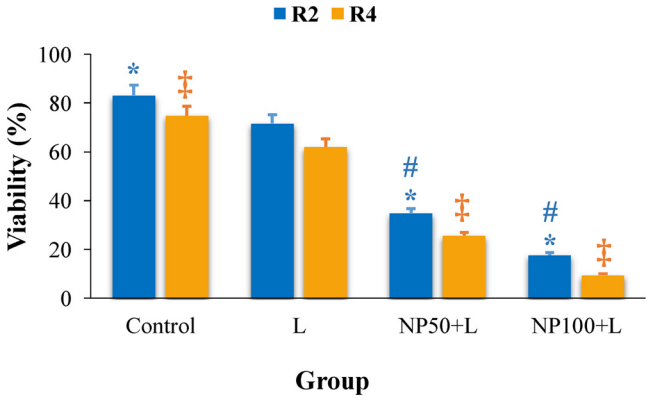

Fig. 4. Viability of KB cells received various treatments in combination with X-ray. Control in this figure stands for the cells which only irradiated with either 2 Gy (R2) or 4 Gy (R4). "L" stands for laser group. Data are shown as the Mean ± SE. (** and ‡ show P- value < 0.001 and # shows P-value < 0.05).

amount of Au content. We observed that 0.15 ng Au was entered into each cell following the incubation of 100μM of NPs with KB cells for 4 h.

3.6. Ultrastructural features of treated KB cells

Treated KB cells were studied by TEM to determine how their ultrastructural features are changed due to treatment with combination therapy (NPs + Laser + RT). Fig. 5(a) shows the TEM micrographs of the cells incubated with NPs and did not receive any kind of exposure, wherein the presence of NPs inside the mitochondria, cytoplasm, and nucleus is easily observable. Fig. 5(b) shows the TEM micrographs of treated cells in which the presence of NPs are detectable. Moreover, massive cell injury can be detected in the treated KB cells, such as disruption of plasma membrane, chromatin condensation, damaged mitochondria and swelling of nucleus membrane.

3.7. Clonogenic assay

Colony formation assay or clonogenic assay is known as an in vitro assay method to determine the cell survival based on the ability of a single cell to grow into a colony. To evaluate this ability of the treated cells, we performed clonogenic survival assay. A significant decrease ($p < 0.001$) was found in surviving fraction of the KB cells irradiated by X-ray after treating with the Au@Fe2O3 NPs and laser compared to those KB cells which only received X-ray radiation (Fig. 6).

3.8. qRT- PCR results

The A260/A280 and A260/A230 of the RNA samples were measured by Nanodrop and these ratios were greater than 2, which met the need for RNA extraction (Table 2).

Expression of the Bax, Bcl2 and HSP70 genes in KB cells treated with NPs, laser, and X-ray, was measured by qRT-PCR. It was found that the expressions of Bax and HSP70 were upregulated while Bcl2 expression was downregulated following the combination therapy. In other words, our results indicated that NPs in combination with laser and/or X-ray induced more expression of intracellular apoptotic genes and significantly inhibited the expression of anti-apoptotic genes. The results are shown in Figs. 7 and 8.

The correlation between cell viability and apoptotic gene expression was examined using the Pearson correlation test. The Pearson correlation coefficient for cell viability and Bax expression was -0.952, showing that the overexpression of Bax genes induces more cell death. For cell viability and Bcl2 expression, the Pearson correlation coefficient was obtained of 0.897, showing a direct correlation between cell viability and Bcl2 gene expression. This means that an increase in Bcl2 gene expression increases cell death.

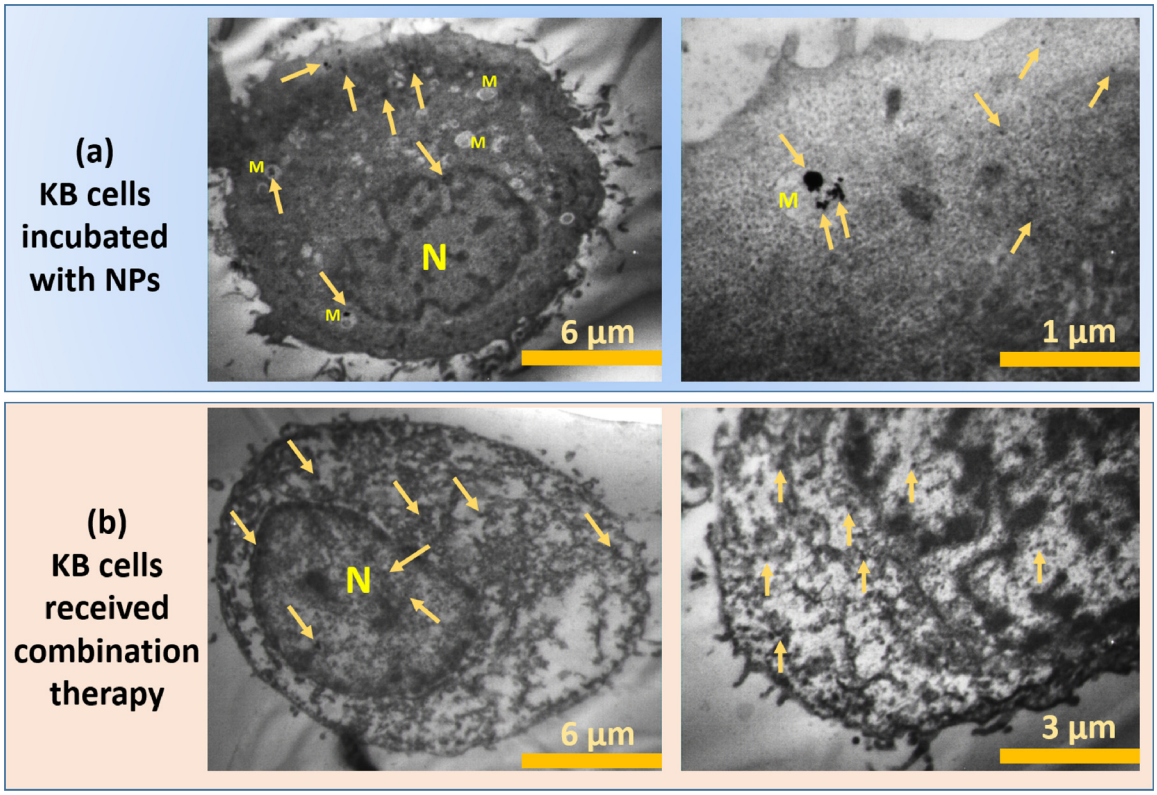

Fig. 5. (a) The results of cellular uptake assay for the synthesized nanoparticles. The arrows show nanoparticles inside the cells. (b) Ultrastructure of the cells after treating with combination therapy. "N" and "M" stands for nucleus and mitochondria of the cells.

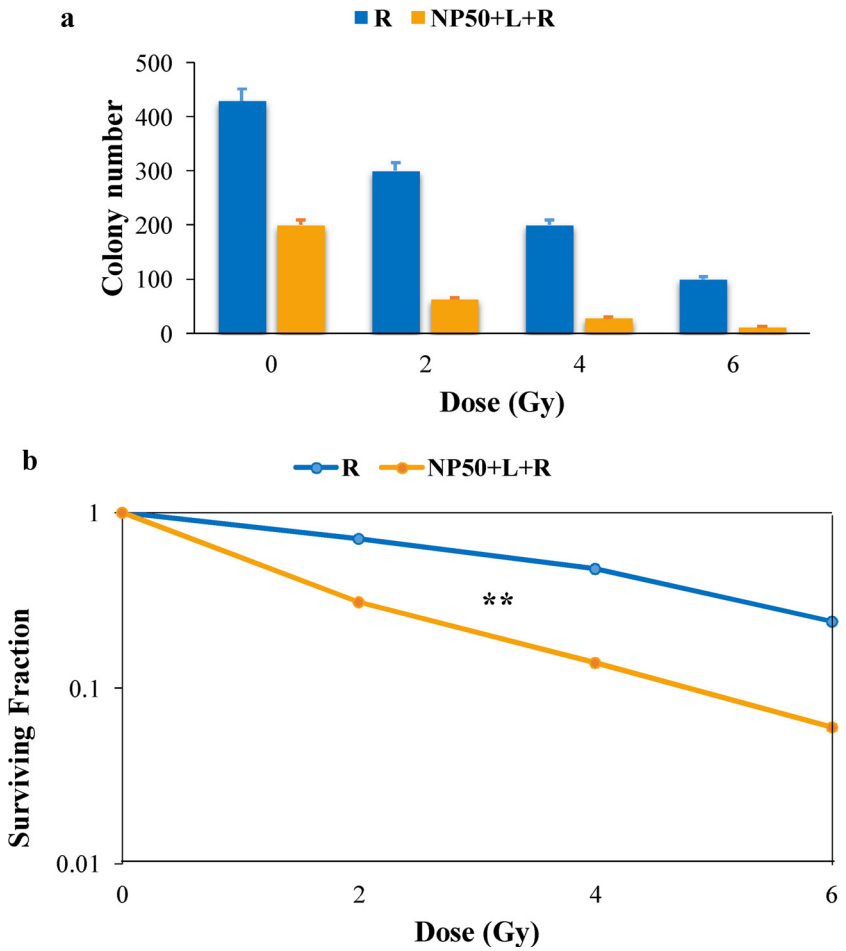

Fig. 6. The results of clonogenic assay for KB cells treated with radiation doses of 0, 2, 4, and 6 Gy in the presence and absence of Laser + NPs (** P- value < 0.001; differences between all groups were significant).

Table 2
RNA concentration and purity in various groups.

Group	ng/μL	A260/A280	A260/A230
Control	353	2.09	2.25
NPs	166	2.06	2.16
Laser	184.4	2.07	2.27
NPs + Laser	100	2.05	2.22
X-ray (2Gy)	242.2	2.09	2.15
Laser + X-ray (2Gy)	220	2.08	2.26
NPs + Laser + X-ray (2Gy)	67.7	2.06	2.11
X-ray (4Gy)	273	2.09	2.28
Laser + X-ray (4Gy)	229	2.08	2.21
NPs + Laser + X-ray (4Gy)	139	2.05	2.25

4. Discussion

Cancer is one of the leading cause of death in the world. Due to the limitations of current cancer treatment methods, it is important to develop low-risk treatment modalities [19]. The combination of PTT and RT may increase the damage to cancer cells, while the harmful effects on normal tissues are kept at the lowest level [20,21]. It is also assumed that nanoparticles are able to enhance the therapeutic ratio of PTT and RT. Albanese and Zhang showed that the highest uptake level for nanoparticles is occurred when their size is ranged from 20 to 60 nm [22,23]. The NPs used in this study had a mean diameter of 40 nm. Consequently, it may be stated that the synthesized NPs had no significant problem in internalization into the KB cancer cells (as confirmed in our ICP and TEM studies). The synthesized NPs showed little cytotoxicity on HGF cells, so it can be stated these NPs have good biocompatibility. Also, at the concentrations of 50 and 100 μM, low toxicity was obtained on KB cells, but cell viability decreased to 54.41 % at the concentration of 150 μM. In fact, increasing the concentration of NPs results in greater adhesion of the NPs to the cell membrane. It may be stated that the entrance of NPs into the cytoplasm and its interaction with organelles caused cell death [24]. When a metal NP is irradiated by light, the free electrons begin to vibrate in the conduction band and SPR is begun [25]. An advantage of core-shell NPs on spherical NPs is that the SPR of the core-shell NPs can be modified to fall into the NIR region. These types of NPs are therefore suitable for the treatment of deep tumors using PTT modality [26,27]. Hirsch used an NIR laser to study the PTT effects of gold nanoshells, for the first time. The breast cancer cells were irradiated for 4 min with a laser at the wavelength of 820 nm. No significant cell death was observed, but the combination of NPs and laser caused severe cell damage [28].

In this study, KB cells were firstly exposed by an 808 nm laser. The MTT test showed that only 5.29 % of the laser treated cells died. However, when treating cells with both laser and NPs, greater cell death rate was observed. After incubation of the cells with NPs at concentrations of 50, 100 and 150 μM for 4 h and then exposure to the 808 nm laser, the KB cell viability was respectively reduced to 68.49 %, 44.74 % and 42.79 %. It can be therefore said that the laser without photosensitizer does not cause much cell death. However, in the presence of NPs, the laser light is converted into heat, causing severe damage to the cell membrane and cell integrity [25]. Ghaznavi et al. reported that exposure of KB and MCF-7 cancer cells by an NIR laser for 10 min did not induce significant cell death. However, core-shell NPs at

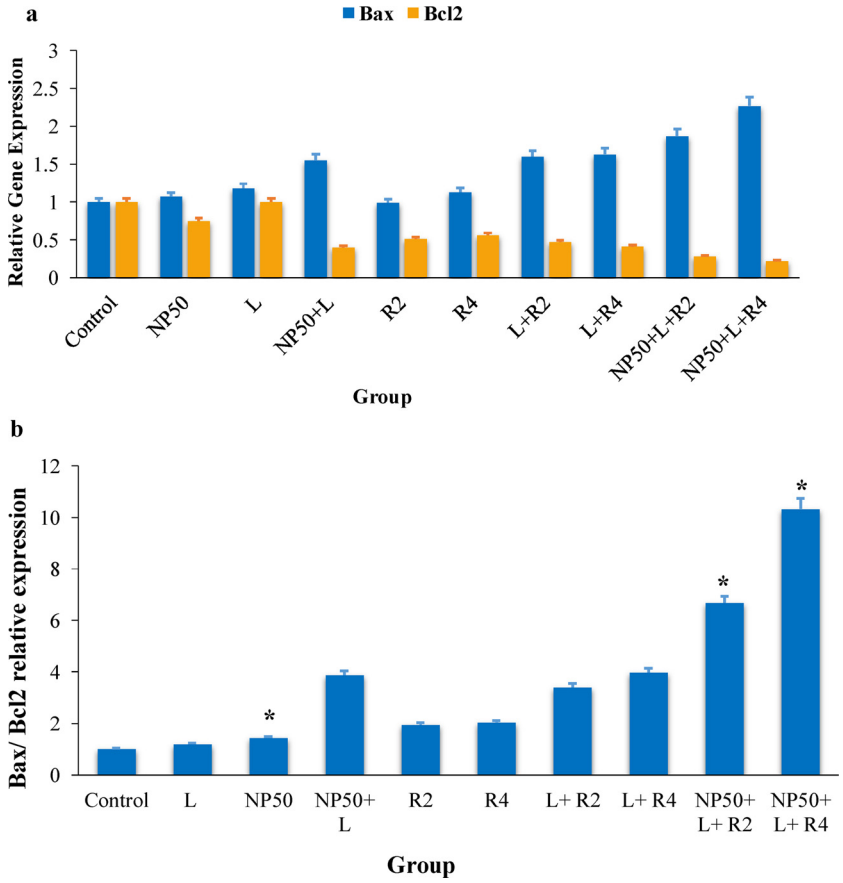

Fig. 7. (a) The status of Bax and Bcl2 relative expression and (b) Bax/Bcl2 relative expression in various treatment groups (data are shown as the Mean ± SE and * means P- value < 0. 05).

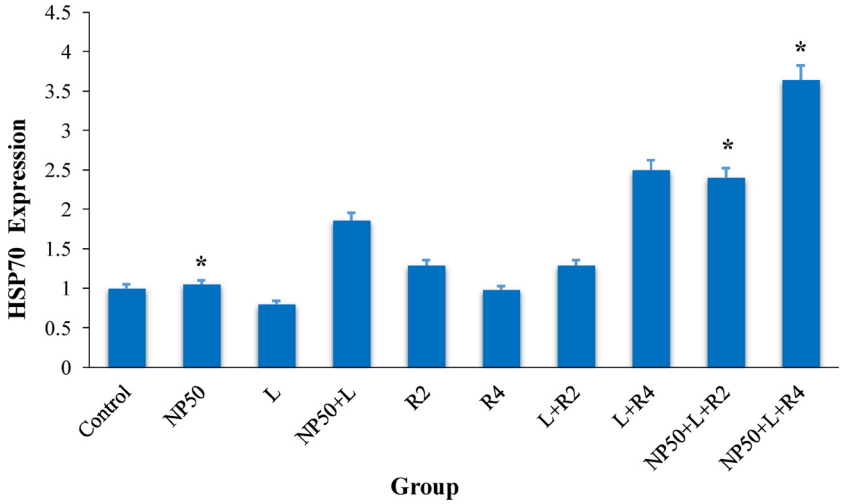

Fig. 8. The status of HSP70 expression in various treatment groups (data are shown as the Mean ± SE and * means P- value < 0.05).

the concentration of 50 μg/ml in combination with laser light caused 62 % and 33 % cell death in the KB and MCF-7 cell lines, respectively [29]. The same results are reported by Mehdizadeh et al. [30], Zhou et al. [31], Hu et al. [32], and Zeinizadeh [33].

The present study also aimed to investigate the radiosensitizing properties of the synthesized NPs in combination with PTT. Our results obtained from colony assay showed that the synthesized core-shell NPs are good radiosensitizers due to presence of a high Z material (Au) and consequently due to an enhancement of X-ray absorbed dose. MTT assay also showed that only 16.75 % death was measured in the KB cells treated with X-ray (2 Gy). The combination of PTT and RT (2 Gy) caused cell death of 65.08 % and 82.18 % at the NPs concentrations of 50 and 100 μM. These results suggest that NPs can enhance the combinatorial anti-cancer effects of PTT and RT. The production of ROS, induction of oxidative stress and inhibition of DNA repair may highly sensitize the resistant KB cells. Several studies showed that RT and PTT are well suited as the complementary methods of cancer treatment [10,34]. Ma et al. studied the effects of PTT and RT on the KB cell line. Incubation of cells with gold nanospike (54 nm) and subsequent irradiation with 808 nm laser for 10 min induced 11 % cell death. The

combination of NPs and RT (6 MV X-ray) reduced cell viability to 54 %, while the combination of PTT and RT reduced cell viability to 40 %, indicating that gold nanospikes were appropriate radiosensitizers [35]. Accordingly, there is good agreement between our results and what reported by other researchers.

We have also studied the alteration of Bax, Bcl2 and HSP70 genes expression following the suggested combination therapy method. It is well-known that Bax and Bcl2 genes regulate apoptosis [36]. Our results showed that Bax expression was not significantly altered in the groups treated with NPs and lasers and X-ray, but it was increased in the combination groups and also Bcl2 expression was downregulated in such groups. The ratio of Bax/Bcl2 is also an index to determine if any given treatment modality is able to induce cell apoptosis [37]. The significant increase in the ratio of Bax/Bcl2 in our study showed that $Au@Fe_2O_3$ NPs coupled with NIR and X-ray exposure highly induce apoptosis in KB cells. Fig. 7(b) shows that the highest level of apoptosis occurred in cells treated with NPs + Laser + RT. So, it can be stated that accumulation of NPs in mitochondria, as shown in Fig. 5, in combination with laser and RT can activate apoptotic genes causing apoptosis and consequently extensive cell death is occurred. Moreover, HSP70 is an important protein and its expression is increased in the stress states. For example, HSP70 gene is overexpressed when a cell experiences heating, inflammation, oxidative stress, cytotoxic agents or radiation [36,38]. Overexpression of HSP70 was seen due to laser irradiation and this effect was further increased when the cells received combination therapy (Fig. 8). Yan et al. had studied the therapeutic effects of magnetic hyperthermia using Fe_2O_3 NPs on SMMC-7721 liver cancer cells. RT-PCR results showed high expression of HSP70 and Bax and a little effect on Bcl2 expression [39]. Similar results were found in the studies reported by Yang [40], Zheng [41], Zhou [42] and there are good agreement between our results and what reported by them.

5. Conclusion

In summary, we showed that the $Au@Fe_2O_3$ core-shell NPs have cytotoxicity for cancer cells and this is while they can be considered as the biocompatible NPs for healthy cells. Our results also showed that $Au@Fe_2O_3$ NP is a good photosensitizing and radiosensitizing agent. More importantly, the combination of PTT and RT in the presence of $Au@Fe_2O_3$ NPs caused significant cell death. In this study, we found massive injury occurred for cell structure and high level of apoptosis may be the reasons of extensive cell death which we observed following the NP assisted photo-thermo-radiotherapy procedure. Accordingly, it may be stated that $Au@Fe_2O_3$ core-shell NP is an appropriate photo-radio-sensitizing nano-agent capable to reduce the dose of X-ray needed to eradicate cancer cells and consequently normal tissue complications may be highly reduced.

Declaration of Competing Interest

None.

Acknowledgements

All supports received from Zahedan University of Medical Sciences (ZaUMS) and Shiraz University of Medical Sciences (SUMS) are acknowledged.

References

[1] H. Zhang, H. Wu, J. Wang, Y. Yang, D. Wu, Y. Zhang, Y. Zhang, Z. Zhou, S. Yang, Graphene oxide-BaGdF5 nanocomposites for multi-modal imaging and photothermal therapy, Biomaterials 42 (2015) 66–77.
[2] M. Babaei, M. Ganjalikhani, A systematic review of gold nanoparticles as novel cancer therapeutics, Nanomed. J. 1 (2014) 211–219.
[3] E. Porcel, O. Tillement, F. Lux, P. Mowat, N. Usami, K. Kobayashi, Y. Furusawa, C. Le Sech, S. Li, S. Lacombe, Gadolinium-based nanoparticles to improve the hadrontherapy performances, Nanomedicine 10 (8) (2014) 1601–1608.
[4] J.F. Hainfeld, F.A. Dilmanian, D.N. Slatkin, H.M. Smilowitz, Radiotherapy enhancement with gold nanoparticles, J. Pharm. Pharmacol. 60 (2008) 977–985.
[5] S. Shrestha, L. Cooper, O. Andreev, Y. Reshetnyak, M. Antosh, Gold nanoparticles for radiation enhancement in vivo, J. Radiat. Oncol. 3 (2016) 26.
[6] J. Beik, M. Jafariyan, A. Montazerabadi, A. Ghadimi-Daresajini, P. Tarighi, A. Mahmoudabadi, H. Ghaznavi, A. Shakeri-Zadeh, The benefits of folic acid-modified gold nanoparticles in CT-based molecular imaging: radiation dose reduction and image contrast enhancement, Artif. Cells Nanomed. Biotechnol. 46 (8) (2017) 1993–2001.
[7] S. Rockwell, I.T. Dobrucki, E.Y. Kim, S.T. Marrison, V.T. Vu, Hypoxia and radiation therapy: past history, ongoing research, and future promise, Curr. Mol. Med. 9 (4) (2009) 442–458.
[8] J.A. Schwartz, R.E. Price, K.L. Gill-Sharp, K.L. Sang, J. Khorchani, B.S. Goodwin, J.D. Payne, Selective nanoparticle-directed ablation of the canine prostate, Lasers Surg. Med. 43 (3) (2011) 213–220.
[9] A. Shakeri-Zadeh, H. Eshghi, G. Mansoori, A. Hashemian, Gold nanoparticles conjugated with folic acid using mercaptohexanol as the linker, J. Nanotechnol. Progress Int. 1 (2009) 13–23.
[10] J. Beik, M. Khateri, Z. Khosravi, S.K. Kamrava, S. Kooranifar, H. Ghaznavi, A. Shakeri-Zadeh, Gold nanoparticles in combinatorial cancer therapy strategies, Coord. Chem. Rev. 387 (2019) 299–324.
[11] Q. Xiao, X. Zheng, W. Bu, W. Ge, S. Zhang, F. Chen, H. Xing, Q. Ren, W. Fan, K. Zhao, A core/satellite multifunctional nanotheranostic for in vivo imaging and tumor eradication by radiation/photothermal synergistic therapy, J. Am. Chem. Soc. 135 (35) (2013) 13041–13048.
[12] V. Hosseini, M. Mirrahimi, A. Shakeri-Zadeh, F. Koosha, B. Ghalandari, S. Maleki, A. Komeili, S.K. Kamrava, Multimodal cancer cell therapy using Au@ Fe2O3 core–shell nanoparticles in combination with photo-thermo-radiotherapy, Photodiagnosis Photodyn. Ther. 24 (2018) 129–135.
[13] C.S. Kumar, F. Mohammad, Magnetic nanomaterials for hyperthermia-based therapy and controlled drug delivery, Adv. Drug Deliv. Rev. 63 (9) (2011) 789–808.
[14] G. Huang, H. Chen, Y. Dong, X. Luo, H. Yu, Z. Moore, E.A. Bey, D.A. Boothman, J. Gao, Superparamagnetic iron oxide nanoparticles: amplifying ROS stress to improve anticancer drug efficacy, Theranostics 3 (2) (2013) 116.
[15] P. Wust, B. Hildebrandt, G. Sreenivasa, B. Rau, J. Gellermann, H. Riess, R. Felix, P.M. Schlag, Hyperthermia in combined treatment of cancer, Lancet Oncol. 3 (2002) 487–497.
[16] W.I. Wei, J.S. Sham, Nasopharyngeal carcinoma, Lancet 365 (9476) (2005) 2041–2054.
[17] S.L. Wolden, W.C. Chen, D.G. Pfister, D.H. Kraus, S.L. Berry, M.J. Zelefsky, Intensity-modulated radiation therapy (IMRT) for nasopharynx cancer: update of the Memorial Sloan-Kettering experience, Int. J. Radiat. Oncol. Biol. Phys. 64 (1) (2006) 57–62.
[18] M. Mirrahimi, M. Khateri, J. Beik, F.S. Ghoreishi, A.S. Dezfuli, H. Ghaznavi, A. Shakeri-Zadeh, Enhancement of chemoradiation by co-incorporation of gold nanoparticles and cisplatin into alginate hydrogel, J. of Biomed. Mater. Res. Part B: App. Biomater. 107 (2019) 2658–2663.
[19] T. Hehr, P. Wust, M. Bamberg, W. Budach, Current and potential role of thermo-radiotherapy for solid tumours, Oncol. Res. Treat. 26 (3) (2003) 295–302.
[20] H. Yonghong, Author's reply to Paulides' commentary on developing effective hyperthermia application for nasopharyngeal cancer, Int. J. Hyperth. 27 (5) (2011) 526-526.
[21] N.G. Huilgol, S. Gupta, C. Sridhar, Hyperthermia with radiation in the treatment of locally advanced head and neck cancer: a report of randomized trial, J. Cancer Res. Ther. 6 (4) (2010) 492.
[22] A. Albanese, P.S. Tang, W.C. Chan, The effect of nanoparticle size, shape, and surface chemistry on biological systems, Annu. Rev. Biomed. Eng. 14 (2012) 1–16.
[23] S. Zhang, J. Li, G. Lykotrafitis, G. Bao, S. Suresh, Size-dependent endocytosis of nanoparticles, Adv. Mater. 21 (4) (2009) 419–424.
[24] R. Wahab, M.A. Siddiqui, Q. Saquib, S. Dwivedi, J. Ahmad, J. Musarrat, A.A. Al-Khedhairy, H.-S. Shin, ZnO nanoparticles induced oxidative stress and apoptosis in HepG2 and MCF-7 cancer cells and their antibacterial activity, Colloids Surf. B Biointerfaces 117 (2014) 267–276.
[25] A. Hashemian, H. Eshghi, G. Mansoori, A. Shakeri-Zadeh, A. Mehdizadeh, Folate-conjugated gold nanoparticles (synthesis, characterization and design for cancer cells nanotechnology-based targeting), Int. J. of Nanosci. and Nanotechnol. 5 (2009) 25–34.
[26] X. Huang, M.A. El-Sayed, Gold nanoparticles: optical properties and implementations in cancer diagnosis and photothermal therapy, J. Adv. Res. 1 (1) (2010) 13–28.
[27] Z. Qin, J.C. Bischof, Thermophysical and biological responses of gold nanoparticle laser heating, Chem. Soc. Rev. 41 (3) (2012) 1191–1217.
[28] L.R. Hirsch, R.J. Stafford, J. Bankson, S.R. Sershen, B. Rivera, R. Price, J.D. Hazle, N.J. Halas, J.L. West, Nanoshell-mediated near-infrared thermal therapy of tumors under magnetic resonance guidance, Proc. Natl. Acad. Sci. 100 (23) (2003) 13549–13554.
[29] A. Montazerabadi, J. Beik, R. Irajirad, N. Attaran, S. Khaledi, H. Ghaznavi, A. Shakeri-Zadeh, Folate-modified and curcumin-loaded dendritic magnetite nanocarriers for the targeted thermo-chemotherapy of cancer cells, Artif. Cells Nanomed. Biotechnol. 47 (2019) 330–340.
[30] M. Mirrahimi, Z. Abed, J. Beik, I. Shiri, A.S. Dezfuli, V.P. Mahabadi, S.K. Kamrava, H. Ghaznavi, A. Shakeri-Zadeh, A thermo-responsive alginate nanogel platform co [HYPHEN]loaded with gold nanoparticles and cisplatin for combined cancer chemo-photothermal therapy, Pharmacol. Res. 143 (2019) 178–185.
[31] Z. Zhou, Y. Sun, J. Shen, J. Wei, C. Yu, B. Kong, W. Liu, H. Yang, S. Yang, W. Wang,

Iron/iron oxide core/shell nanoparticles for magnetic targeting MRI and near-infrared photothermal therapy, Biomaterials 35 (26) (2014) 7470–7478.
[32] Y. Hu, R. Wang, S. Wang, L. Ding, J. Li, Y. Luo, X. Wang, M. Shen, X. Shi, Multifunctional Fe 3 O 4@ Au core/shell nanostars: a unique platform for multimode imaging and photothermal therapy of tumors, Sci. Rep. 6 (2016) 28325.
[33] E. Zeinizade, M. Tabei, A. Shakeri-Zadeh, H. Ghaznavi, N. Attaran, A. Komeili, B. Ghalandari, S. Maleki, S.K. Kamrava, Selective apoptosis induction in cancer cells using folate-conjugated gold nanoparticles and controlling the laser irradiation conditions, Artif. Cells Nanomed. Biotechnol. 46 (2018) 1026–1038.
[34] R. Hu, M. Zheng, J. Wu, C. Li, D. Shen, D. Yang, L. Li, M. Ge, Z. Chang, W. Dong, Core-shell magnetic gold nanoparticles for magnetic field-enhanced radio-photothermal therapy in cervical Cancer, Nanomaterials 7 (5) (2017) 111.
[35] N. Ma, Y.-W. Jiang, X. Zhang, H. Wu, J.N. Myers, P. Liu, H. Jin, N. Gu, N. He, F.-G. Wu, Enhanced radiosensitization of gold nanospikes via hyperthermia in combined Cancer radiation and photothermal therapy, ACS Appl. Mater. Interfaces 8 (2016) 28480–28494.
[36] L. Bian, Y. He, X. Liang, S. Wang, Apoptosis induced by hyperthermia and the expressions of Bcl-2 and Bax proteins in maxillofacial squamous cell carcinomas, J. Oral Sci. Res. 19 (6) (2003) 448–450.
[37] L. Bian, Y. He, X. Liang, S. Wang, Apoptosis induced by hyperthermia and the expressions of Bcl-2 and Bax proteins in maxillofacial squamous cell carcinomas, J. Oral Sci. Res. 19 (2003) 448–450.
[38] P. Schildkopf, B. Frey, O.J. Ott, Y. Rubner, G. Multhoff, R. Sauer, R. Fietkau, U.S. Gaipl, Radiation combined with hyperthermia induces HSP70-dependent maturation of dendritic cells and release of pro-inflammatory cytokines by dendritic cells and macrophages, Radiother. Oncol. 101 (1) (2011) 109–115.
[39] S.Y. Yan, M.M. Chen, J.G. Fan, Y.Q. Wang, Y.Q. Du, Y. Hu, L.M. Xu, Therapeutic mechanism of treating SMMC-7721 liver cancer cells with magnetic fluid hyperthermia using Fe2O3 nanoparticles, Braz. J. Med. Biol. Res. 47 (2014) 947–959.
[40] L. Yang, Y.-T. Tseng, G. Suo, L. Chen, J. Yu, W.-J. Chiu, C.-C. Huang, C.-H. Lin, Photothermal therapeutic response of cancer cells to aptamer–gold nanoparticle-hybridized graphene oxide under NIR illumination, ACS Appl. Mater. Interfaces 7 (9) (2015) 5097–5106.
[41] Q. Zheng, H. Yang, J. Wei, J.-l. Tong, Y.-q. Shu, The role and mechanisms of nanoparticles to enhance radiosensitivity in hepatocellular cell, Biomed. Pharmacother. 67 (7) (2013) 569–575.
[42] C.-d. Zhu, Q. Zheng, L.-x. Wang, H.-F. Xu, J.-l. Tong, Q.-a. Zhang, Y. Wan, J.-q. Wu, Synthesis of novel galactose functionalized gold nanoparticles and its radiosensitizing mechanism, J. Nanobiotechnol. 13 (1) (2015) 67.